Power Delay Profile Analysis and Modeling of Industrial Indoor Channels

Yun Ai[1,2], Michael Cheffena[1], Qihao Li[1,2]
[1]Faculty of Technology, Economy and Management, Norwegian University of Science and Technology, Norway
[2]Faculty of Mathematics and Natural Sciences, University of Oslo, Norway
Email: {yun.ai, michael.cheffena, qihao.li}@ntnu.no

***Abstract*—In this paper, power delay profile (PDP) measurements of three different industrial indoor environments are presented. The measurements were performed in the frequency range of 800 MHz to 2.7 GHz using a vector network analyzer (VNA) and the virtual antenna array method. Dense multipath scattering with multipath components arriving in clusters was observed. This is due to the abundance of highly reflective scatterers present in the measured industrial environments. The measurement results reveal two different shapes of PDP, neither of which fully fits the well known Saleh-Valenzuela (S-V) model or power-law model. Thus, modifications were made on the conventional S-V model and power-law model to better represent the measurement results. Furthermore, Weibull distribution was found to fit the measured small-scale fading.**

***Index Terms*—Channel measurement, power delay profile, multipath propagation, statistical model, industrial environment.**

I. Introduction

Wireless technologies have gained increasing attention from manufacturing factories due to their potential in enabling remote control, data collection and automation to improve the efficiency and productivity of industrial facilities. However, industrial environments often feature harsh propagation characteristics (e.g., high noise level, intensive interferences, etc), which can possibly cause considerable impairments to mission-critical signals. Thus, understanding the behavior of industrial channel is vital for the design and evaluation of robust wireless systems for industrial applications [1]–[3].

In this work, we present wideband measurement results of industrial environments from 0.8 to 2.7 GHz which covers the frequency bands allocated for industrial wireless communication systems [4]. An analysis of the channel impulse response is presented. Based on our analysis, we find that the trend of cluster power decay is not in accordance with the assumption of Saleh-Valenzuela (S-V) model [5] and the ray power decay reveals two different power delay profile (PDP) shapes. Thus, modifications on the S-V model and power-law model were made to accurately model the measurements.

The remainder of the paper is organized as follows: Section II illustrates the measurement setup and environments followed by a description of data processing. Measurement results and discussions are presented in Section III. A detailed description of the models and the extraction of model parameters based on our measurements is given in Section IV. Finally, summary and conclusion are drawn in Section V.

II. Wideband Measurement

A. Environment Description

Observations from a large number of modern factories show that there are some physical characteristics common to most industrial environments. The industrial buildings are generally taller than ordinary office buildings and are sectioned into several working areas. Between the working areas, there are usually straight aisles for passing people or materials. Modern factories usually have perimeter walls made of concrete or steel and the ceilings are often made of metal and supported with intricate metal supporting trusses. In addition to above common characteristics, the object type and density within specific industrial environment may vary and play an important role in characterizing the channel.

Measurements presented in this paper were performed in the assembly shop, electronics room and mechanical room of an electronics manufacturing factory in Gjøvik, Norway. All three rooms share the aforementioned physical characteristics. The assembly shop covers an area of about $15 \times 17\ \mathrm{m}^2$ with a height of around 5 meters. It houses two long work desks with three aisles along the longer dimension. Several big racks are placed along the aisle to put assembly components and a big metallic shelf holding manufacturing items is placed against the wall (see Fig. 1a). The electronics room is slightly bigger with an area of $18 \times 27\ \mathrm{m}^2$ and a height of around 5 meters. It houses two rows of medium-size machinery with a lot of metallic valves present (see Fig. 1b). The mechanical room is about $20{\times}30\ \mathrm{m}^2$ in size and around 6 meters in height. It has several big metallic machines but is less occupied than the electronics room. Several pipes are placed off the roof and a big shelf holding manufacturing components is placed against one wall (see Fig. 1c).

B. Measurement Setup

The vector network analyzer (VNA) measures S_{21} parameter, which allows the extraction of the complex channel transfer function $H(f)$ for the measured frequency range (800 MHz to 2.7 GHz in our measurements). 600 points were taken within the measured frequency band, i.e, about 3.21 MHz between two adjacent frequency points. This configuration results in a delay resolution of about 0.526 ns and a maximum resolvable delay of around 320 ns. The swept-frequency signal generated by the VNA was transmitted by an omnidirectional, vertically polarized broadband transmitting antenna (Tx)

(a) Assembly room (b) Electronics room (c) Mechanical room

Fig. 1: Industrial measurement environments.

placed 1.8 meters above the ground and received by a receiving antenna (Rx) of the same type and height. The Rx was placed 10-18 meters away from the Tx for different measurements.

The virtual uniform linear antenna array (ULA) method was used in the channel transfer function measurement. The Tx was moved along a linear array of $M = 5$ elements and the Rx was move along an uniform rectangular array consisting of $N = 3 \times 6$ elements (see Fig. 2). With such a setup, a virtual multiple-input-multiple-output (MIMO) system of 5 by 18 antennas was created. In order to obtain independent fading for different elements of the virtual array, the separation between adjacent elements was set to 18.75 cm, corresponding to half a wavelength at 800 MHz. Altogether, four ULA measurements were conducted in the three rooms (line-of-sight (LOS) measurement in all rooms as well as a non-line-of-sight (NLOS) measurement in the electronics room).

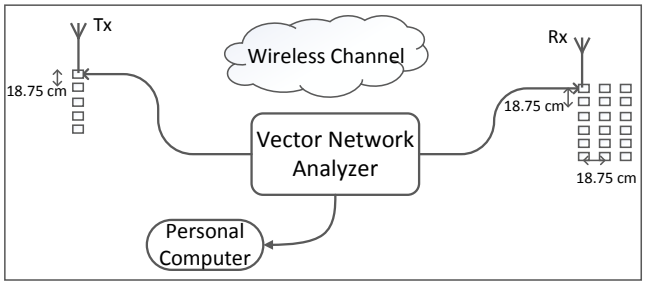

Fig. 2: Measurement setup.

C. Measurement Data Processing

After obtaining the frequency-domain channel transfer function between m-th element of the Tx array and n-th element of the Rx array, $H(f, m, n)$, the channel transfer function is filtered by a Hanning window h_w to reduce aliasing. Next it is converted to the delay domain using Inverse Discrete Fourier Transform (IDFT) and leads to an instantaneous PDP, $\mathrm{PDP}(\tau, m, n)$, which we will refer to as local PDP hereinafter. This process is mathematically expressed as

$$\mathrm{PDP}(\tau, m, n) = \left| \frac{1}{N_f} \sum_{n=1}^{N_f} [H(f, m, n) \times h_w] \exp(j2\pi f_n \tau) \right|^2, \quad (1)$$

where N_f is the number of frequency bins.

Finally, all local PDPs are linearly averaged to generate the averaged power delay profile $\mathrm{APDP}(\tau)$:

$$\mathrm{APDP}(\tau) = E[\mathrm{PDP}(\tau, m, n)], \quad (2)$$

where $E\{\cdot\}$ denotes the ensemble average taken over all measured $M \times N$ snapshots.

Prior to averaging, the delay axis of each local PDP is shifted such that the first arriving multipath component (MPC) corresponds to the same delay bin for all local PDPs. This shift facilitates a more accurate extraction of the statistical parameters of the first arriving MPCs from the ensemble average [6].

III. Measurement Results

A. Shapes of the PDPs

Figure 3a and 3b show the APDP of the assembly room and mechanical room measurements under LOS scenario, respectively. Figure 3c and 3d display the APDP of the LOS and NLOS measurements in the electronics room, respectively. We can see that all measured APDPs consist of several clearly identifiable clusters. For the assembly and mechanical room measurements, the ray decay within each cluster follows an exponential relationship with delay, which translates into a linear dependence when the received power is in dB scale. However, for the electronics room measurements, it is seen that the exponential decay assumed by the S-V model cannot fit the ray decay well and power-law decay seems a better representation. Power-law ray decay has also been reported in previous measurements of various environments, e.g., a hospital room in [7], an industrial facility in [8], etc.

In terms of cluster decay, the original S-V model also assumes a linear dependence between the power in dB versus delay. However, that is not the case in our measurements. The cluster decay in our measurements shows a power decrease at a rate inversely proportional to the delay. Thus, a different approach needs to be used to model the cluster decay.

B. Cluster Identification

Currently, there is no formal way of identifying clusters since different researchers can even have different definition or criteria on cluster. In our analysis, we use the 'visual inspection' approach by finding the local maximum and pronounced steps in received power. This approach is sufficient and accurate enough when the clusters are well-separated in the delay domain, which is the case in our measurements and is also widely used by others [8]–[10].

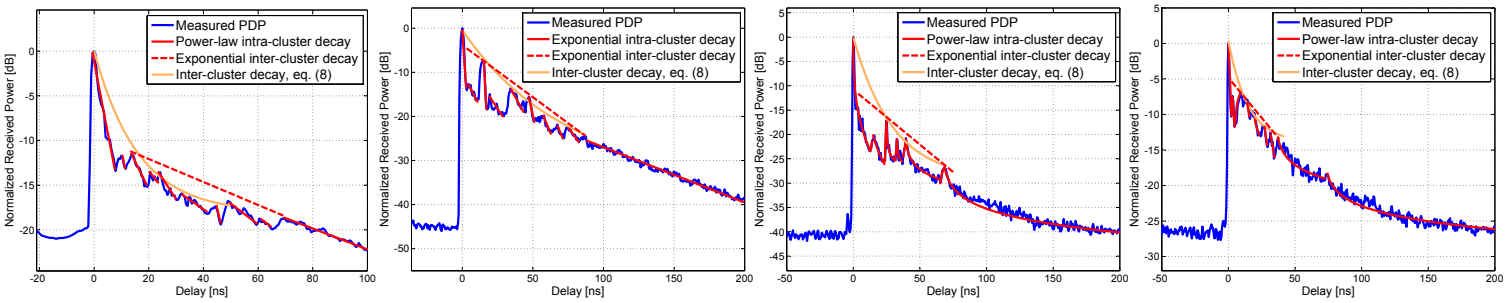

(a) Assembly room, LOS (b) Mechanical room, LOS (c) Electronics room, LOS (d) Electronics room, NLOS

Fig. 3: Measured APDPs in different environments and scenarios.

IV. Modeling

A. The Saleh-Valenzuela Approach

The channel impulse response of S-V model is given by [5]

$$h(\tau) = \sum_{l=1}^{L}\sum_{k=1}^{K_l} g_{kl} e^{j\theta_{kl}} \delta(\tau - T_l - \tau_{kl}) = \sum_{l=1}^{L}\sum_{k=1}^{K_l} \left(\overline{g_{11}^2} e^{-T_l/\Gamma} e^{-\tau_{kl}/\gamma}\right)^{\frac{1}{2}} e^{j\theta_{kl}} \delta(\tau - T_l - \tau_{kl}), \tag{3}$$

where L is the number of clusters, K_l is the number of MPCs in cluster l, g_{kl} and θ_{kl} are the multipath gain coefficient and phase of the kth component in cluster l, respectively. Time instant T_l is the time of arrival (TOA) of the lth cluster and τ_{kl} is the delay of the kth component relative to the time T_l.

With the channel impulse response in (3), the PDP of the S-V model in dB can be expressed as:

$$\mathrm{PDP}(\tau) = \sum_{l=1}^{L}\sum_{k=1}^{K_l} \Bigg[10\log_{10} g_{11}^2 - \underbrace{\frac{T_l}{\Gamma}(10\log_{10} e)}_{\mathrm{P}(T_l)\,[\mathrm{dB}]} - \underbrace{\frac{\tau_{kl}}{\gamma}(10\log_{10} e)}_{\mathrm{P}(\tau_{kl})\,[\mathrm{dB}]} \Bigg] \cdot \delta(\tau - T_l - \tau_{kl}). \tag{4}$$

where the parameters are defined in (3). In (4), the first term is a constant while $\mathrm{P}(T_l)$ and $\mathrm{P}(\tau_{kl})$ represent the cluster decay and ray decay, respectively. A schematic representation of (4) is shown in Fig. 4.

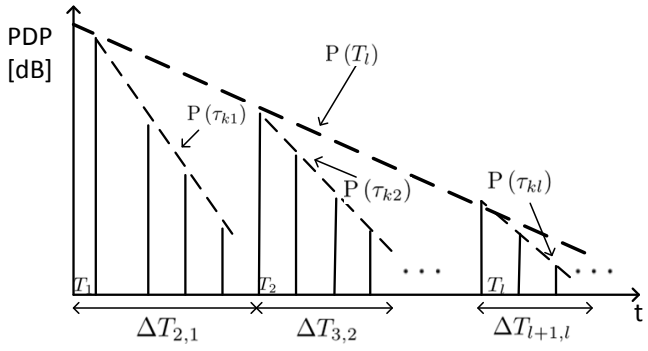

Fig. 4: Schematic representation of the S-V model given in (4).

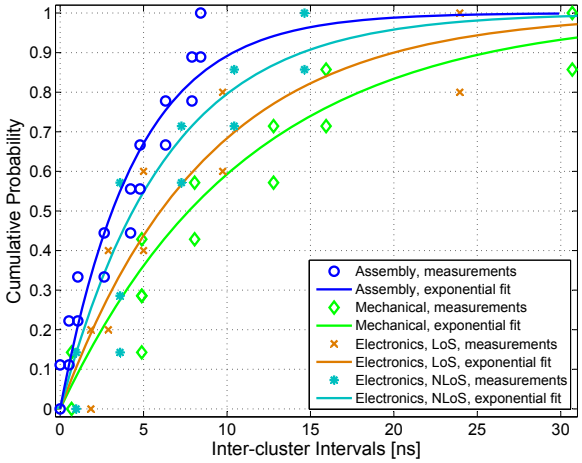

Fig. 5: Distribution of inter-cluster intervals with exponential fitting.

1) Cluster and Ray Arrival Modeling:

The S-V model assumes that clusters arrive according to stochastic Poisson process, which leads to the exponential distributions of inter-cluster duration ($\Delta T_{l,l-1} = T_l - T_{l-1}$):

$$\Pr(\Delta T_{l,l-1}) = \Lambda \cdot \exp[-\Lambda \cdot (\Delta T_{l,l-1} - x_0)], \tag{5}$$

where Λ is the cluster arrival rate and x_0 is an offset.

Figure 5 shows the cumulative distribution functions (CDF) of measured inter-cluster durations, which show a good fitness between the measurements and exponential distributions. With the assumption of $\Delta T_{l,l-1}$ following exponential distribution, the maximum likelihood (ML) estimation of the cluster arrival rate, Λ, can be obtained from: $\hat{\Lambda} = \frac{1}{\overline{\Delta T}}$, where $\overline{\Delta T}$ is the sample mean of all measured inter-cluster durations $\Delta T_{l,l-1}$.

In the S-V model, the arrival of rays is also assumed to be a stochastic Poisson process. But the limited delay resolution of 0.526 ns does not enable us to resolve the inter-path arrival times by an inverse FFT of the measured data, which means that every resolvable delay bin contains non-negligible amount of energy. So we resort to interpreting the S-V model as a classical tapped delay line model: delay taps (rays) are assumed to arrive every 0.526 ns, thus the ray arrival rate being 1.9 GHz.

2) Ray Decay Modeling:

It has been observed and proposed in [8] that the ray power decay constant increases linearly with delay. This is

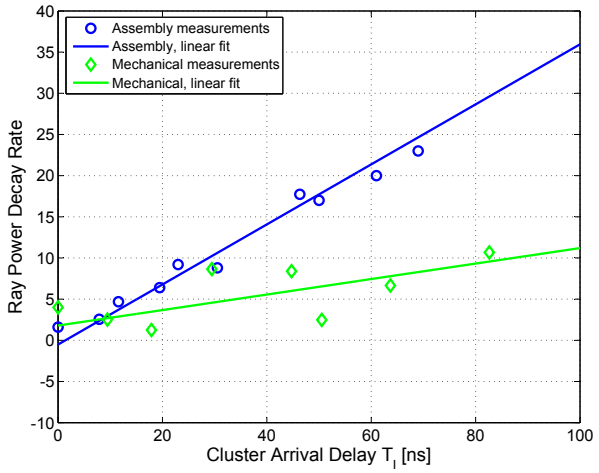

Fig. 6: Ray power decay rates versus cluster delays in assembly room and mechanical room.

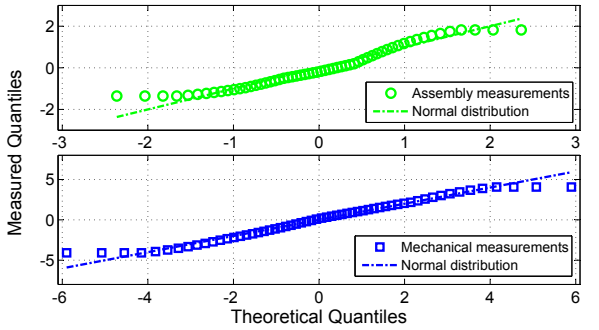

Fig. 7: QQ plot of the random variable $\mathcal{N}_{\sigma_1}$ in (6) versus a Normal distribution.

also the case for our measurements in the assembly shop and mechanical room (see Fig. 6). We extend the model by appending a random variable $\mathcal{N}_{\sigma_1}$:

$$\gamma(T_l) = a \cdot T_l + b + \mathcal{N}_{\sigma_1}, \tag{6}$$

where $\gamma(T_l)$ denotes the ray power decay coefficient for the l-th cluster starting at time instant T_l. Parameter a and b are constants and $\mathcal{N}_{\sigma_1}$ follows a zero-mean Gaussian distribution with standard deviation σ_1 (see Fig. 7). Then we can write the ray power decay $\mathrm{P}(\tau_{kl})$ in (4) as

$$\mathrm{P}(\tau_{kl})\,[\mathrm{dB}] = \frac{\tau_{kl}}{\gamma(T_l)} = \frac{\tau_{kl}}{a \cdot T_l + b + \mathcal{N}_{\sigma_1}}. \tag{7}$$

3) Cluster Decay Modeling:

As discussed in Section III-A, the assumption of the S-V model on cluster decay does not hold for our measurements. By fitting the measurements with various models, it is found that the measured cluster decaying power in dB versus delay can fit well to an exponential decay (see Fig. 3). Similar cluster power decay profiles have also been observed in other reported measurements, e.g., in [7]. Thus, the cluster power decay for the normalized APDP is modeled as

$$\mathrm{P}(T_l)\,[\mathrm{dB}] = c \cdot \exp\left(-\frac{T_l}{d}\right) + e, \tag{8}$$

where c, d and e are model constants. From Fig. 3, we can see that (8) provides a much better fit to the measurements than exponential decay assumed by the conventional S-V model.

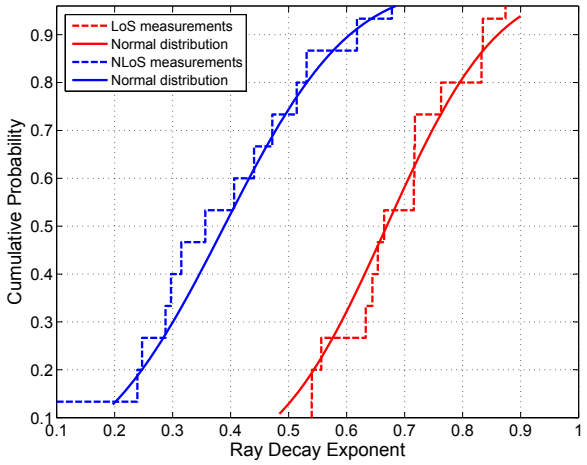

Fig. 8: CDFs of ray power decay rate measurements and Normal distribution in electronics room.

The extracted parameters for the assembly shop and mechanical room using the modified S-V model are listed in Table I.

B. The Power-Law Approach

In the power-law approach, the PDP is modeled as a set of power-law decreases with varying decay factors separated by spectral components (the dominant components determined by cluster power decay). The PDP in dB is given by [6]

$$\mathrm{PDP}(\tau) = \sum_{l=1}^{L}\sum_{k=1}^{K_l}\Big[10\log_{10} g_{11}^2 - \mathrm{P}(T_l) - \underbrace{10 n_l \log_{10}(\tau_{kl})}_{\mathrm{P}(\tau_{kl})\,[\mathrm{dB}]}\Big] \cdot \delta(\tau - T_l - \tau_{kl}), \tag{9}$$

where the first term is a constant, n_l is the ray decay exponent of the l-th cluster and other parameters are defined in (3). The term $\mathrm{P}(T_l)$ represents the cluster power decay in dB and is given in (8).

The cluster and ray arrival rates, T_l and τ_l have already been discussed in Section IV-A1. The ray decay exponent, n_l, in (9) is determined by finding the least-square fit to the PDP in dB for each cluster. Unlike the ray decay factors from the assembly and mechanical room measurements, where it increases linearly with delay (see (6)), it is found that the parameter n_l for $l > 1$ from the electronics room measurements is hardly a function of delay but can be modeled as a Normal random variable (see Fig. 8), i.e.

$$n_l \backsim \mathcal{N}(u, \sigma_2) \qquad l \in [2, L]\,. \tag{10}$$

The ray decay factor for the first cluster, n_1, is excluded because it is associated with the LOS or first dominant path, and the factor is significantly greater than other components.

The extracted parameters for the electronics room using the power-law approach are summarized in Table I.

C. Small-scale Fading Statistics

The small-scale fading characteristic was evaluated with the measurement data from bins at specific excess delays,

TABLE I: Parameters for the Modified S-V Model and Power-law Model

Parameters	Clusters No.	Cluster Arrivals, eq. (5)		Ray Decays, eq. (6) or (10)						Cluster Decays, eq. (8)		
Scenarios	L	$1/\Lambda$ [ns]	x_0	a	b	σ_1	n_1	u	σ_2	c	d	e
Assembly, LOS	10	4.51	3.7	0.36	-0.51	1.11	-	-	-	18.14	16.05	-18.29
Mechanical, LOS	8	14.14	3.0	0.09	1.79	2.78	-	-	-	33.79	72.27	-34.22
Electronics, LOS	6	13.68	5.0	-	-	-	1.89	0.67	0.15	29.23	29.77	-29.29
Electronics, NLOS	8	8.50	2.2	-	-	-	1.48	0.39	0.17	14.28	14.64	-14.40

which were matched to some typical theoretical amplitude fading distributions such as Log-normal, Nakagami, Rician, and Weibull distributions. Hypothesis testing was applied with the chi-squared (χ^2) test at the significance level of 0.05 to elaborate the goodness-of-fit of these distributions [10]–[12]. We characterize the small-scale statistics by fitting the observed amplitudes in each delay bin of all 90 measurements to each of the aforementioned distributions. The variations are treated as stochastic. It was found that the Weibull distribution turns out to have the highest passing rate and is the best fit for the small-scale amplitude statistics (see Table II). Figure 9 shows the comparison between CDFs of various distributions and the measured small-scale fading from the electronics room under LOS scenario at 20 ns and 60 ns path delays. Measurements from the other rooms show similar results.

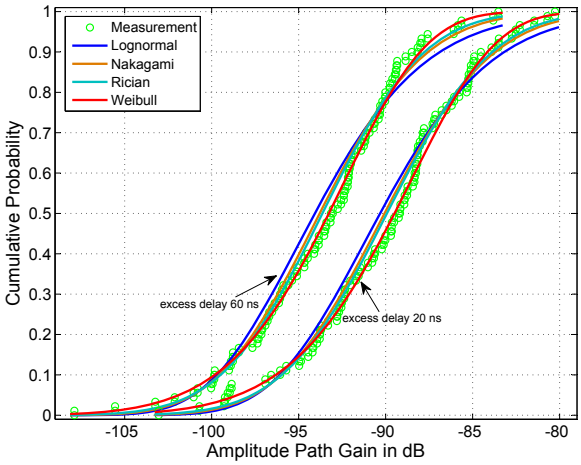

Fig. 9: Small-scale fading CDFs fitted with different distributions at different excess delays in electronics room.

V. Conclusion

In this paper, power delay profile measurements of three different industrial indoor environments were presented. The measurements were performed in the frequency range of 0.8 to 2.7 GHz using frequency-domain channel sounding and virtual antenna array technique.

It was observed that the PDPs clearly exhibited several clustering of the received power as a function of delay. The measurement results revealed two different shapes of the PDP. It was found that the cluster decay in dB scale followed an exponential decay for all measured PDPs. The ray power decay constant γ was found to increase linearly with delay for PDP measurements from the assembly shop and the mechanical room, and an exponential ray power decay with delay was observed for these locations. However, for the electronics room, the ray decay within each cluster can be modeled as a power-law decrease with the ray decay factors γ described by a Normal random variable. The cluster inter-arrival times following the exponential distribution was verified from our measurements. The Weibull distribution was found to fit the small-scale fading of MPCs at different delay taps.

TABLE II: Passing Rates of χ^2 Test at 5% Significance Level

Distributions	Weibull	Lognormal	Nakagami	Ricean
Assembly, LOS	89.8%	52.2%	60.3%	64.2%
Mechanical, LOS	91.3%	47.0%	54.0%	58.5%
Electronics, LOS	93.0%	50.2%	56.8%	58.5%
Electronics, NLOS	92.5%	62.7%	70.7%	74.0%

References

[1] E. Tanghe, D. Gaillot, M. Liénard, L. Martens, and W. Joseph, "Experimental analysis of dense multipath components in an industrial environment," *IEEE Transactions on Antennas and Propagation*, vol. 62, no. 7, pp. 3797–3805, 2014.

[2] P. Stenumgaard, J. Chilo, P. Ferrer-Coll, and P. Angskog, "Challenges and conditions for wireless machine-to-machine communications in industrial environments," *IEEE Communications Magazine*, vol. 51, no. 6, 2013.

[3] J. Karedal, S. Wyne, P. Almers, F. Tufvesson, and A. F. Molisch, "UWB channel measurements in an industrial environment," in *Proc. of IEEE Global Telecommunications Conference*, vol. 6, 2004, pp. 3511–3516.

[4] IEEE 802 LAN/MAN Standards Committee and others, "Wireless LAN medium access control (MAC) and physical layer (PHY) specifications," *IEEE Standard*, vol. 802, no. 11, 1999.

[5] A. Meijerink and A. F. Molisch, "On the physical interpretation of the Saleh-Valenzuela model and the definition of its power delay profiles," *IEEE Transactions on Antennas and Propagation*, vol. 62, no. 9, pp. 4780–4793, 2014.

[6] E. Tanghe, W. Joseph, J. D. Bruyne, L. Verloock, and L. Martens, "The industrial indoor channel: statistical analysis of the power delay profile," *AEÜ-International Journal of Electronics and Communications*, vol. 64, no. 9, pp. 806–812, 2010.

[7] M. Kyro, K. Haneda, J. Simola, K.-i. Takizawa, H. Hagiwara, and P. Vainikainen, "Statistical channel models for 60 GHz radio propagation in hospital environments," *IEEE Transactions on Antennas and Propagation*, vol. 60, no. 3, pp. 1569–1577, 2012.

[8] J. Karedal, S. Wyne, P. Almers, F. Tufvesson, and A. F. Molisch, "A measurement-based statistical model for industrial ultra-wideband channels," *IEEE Transactions on Wireless Communications*, vol. 6, no. 8, pp. 3028–3037, 2007.

[9] A. F. Molisch, J. R. Foerster, and M. Pendergrass, "Channel models for ultrawideband personal area networks," *IEEE Wireless Communications*, vol. 10, no. 6, pp. 14–21, 2003.

[10] L. Betancur, N. Cardona, A. Navarro, and L. Traver, "A statistical channel model for on body area networks in ultra wide band communications," in *LATINCOM'09*. IEEE, 2009, pp. 1–6.

[11] C.-C. Chong and S. K. Yong, "A generic statistical-based UWB channel model for high-rise apartments," *IEEE Transactions on Antennas and Propagation*, vol. 53, no. 8, pp. 2389–2399, 2005.

[12] D. Cassioli and A. Durantini, "Measurements, modeling and simulations of the UWB propagation channel based on direct-sequence channel sounding," *Wireless Communications and Mobile Computing*, vol. 5, no. 5, pp. 513–523, 2005.